Advances in Nano Research, *Vol. 7 No. 5 (2019) 365-377*
DOI: https://doi.org/10.12989/anr.2019.7.5.365

Effectiveness of SWNT in reducing the crack effect on the dynamic behavior of aluminium alloy

Abdellatif Selmi*[1,2]

[1] *Department of Civil Engineering, College of Engineeriwng in Al-Kharj, Prince Sattam bin Abdulaziz University, Al-Kharj 11942, Saudi Arabia*
[2] *Ecole Nationale d'Ingénieurs de Tunis (ENIT), Civil Engineering Laboratory, B.P. 37, Le belvédère 1002, Tunis, Tunisia*

(*Received April 15, 2019, Revised May 18, 2019, Accepted August 7, 2019*)

Abstract. This paper investigates the effectiveness of Single Walled Carbon Nanotubes, SWNT, in improving the dynamic behavior of cracked Aluminium alloy, Al-alloy, beams by using a method based on changes in modal strain energy. Mechanical properties of composite materials are estimated by the Eshelby-Mori-Tanaka method. The influence of SWNT volume fraction, SWNT aspect ratio, crack depth and crack location on the natural frequencies of the damaged 3D randomly oriented SWNT reinforced Al-alloy beams are examined. Results demonstrate the significant advantages of SWNT in reducing the effect of cracks on the natural frequencies of Al-alloy beams.

Keywords: aluminium alloy; crack; SWNT; vibration

1. Introduction

Investigation into the dynamic behavior of cracked Al-alloy beams has aroused continuing interest amongst researchers. This is because the subject matter is of considerable practical importance in engineering design to ensure safety and integrity of load carrying structures that are vulnerable to cracks and other damages. The reduction in the strength and stiffness properties of a structure due to the presence of a single or multiple cracks can be dangerous and may lead to catastrophic structural failures.

Duan *et al*. (2018) investigates the behavior of Al-alloy plates with and without initial cracks under repeated impacts. Different crack lengths and depths have been considered. It was observed that plates with larger cracks carried smaller impact forces and assumed larger deformations. The ultimate strength of structures with initial cracks for thin Al-alloy plates, and for stiffened and unstiffened plates with varied crack position, length and angle between the loading direction and crack was discussed by Seifi and Khoda-yari (2011), Rahbar-Ranji and Zarookian (2015) and Shi *et al*. (2017). The susceptibilities of Al-alloy to solidification crack were studied with trans-varestraint tests and tensile tests at elevated temperature by Liu *et al*. (2006). The results show that the strain rate has different effects on crack susceptibility of Al-alloys. Xing *et al*. (2013) investigated the dynamic fracture behaviors of the extruded Al-alloys by using an instrumented drop tower machine. They pointed out that both the initiation toughness and the propagation toughness increase with the loading rate. Further, the difference between the fracture toughness behaviors is found to be dependent on the fracture mechanism. Different loading conditions are applied by Pedersen *et al*. (2011) in order to identify the fracture mechanisms of Al-alloy. They discussed the influence of stress triaxiality on the fracture behavior through the introduction of a notch in the tensile specimen. Mostafavi *et al*. (2011) investigated the effect of stress state on the fracture of 2024-T361 Al-alloy. Dumont *et al*. (2003) studied the relationship among microstructure, strength and toughness of Al-alloy. They examined the influences of quenching rate and aging treatment on the precipitate microstructure and the associated compromise between yield strength and fracture toughness. Han *et al*. (2011) studied the effects of the pre-stretching and aging on the strength and fracture toughness of 7050 Al-alloy. The results show that the peak-aged 7050 Al-alloy possesses a higher strength, but its fracture toughness is poor. Recently, Borvik *et al*. (2010) investigated the quasi-brittle fracture of AA7075-T651 Al-alloy plate in plate impact test.

SWNT possesses exceptional mechanical, electrical and thermal properties (Shen 2009). They are demonstrated to be capable to improve the dynamic behavior of composite structures. The effect of the SWNT volume fraction and its distribution on the flexural stiffness and the natural frequency of different structural elements are discussed in the literature and found to be very advantageous (Heshmati and Yas 2013, Shenas *et al*. 2017, Yas and Samadi 2012, Nejati *et al*. 2016, Selmi and Bisharat 2018).

Bakhadda *et al*. (2018) examined the vibration and bending response of SWNT reinforced composite plates resting on the Pasternak elastic foundation. The SWNT volume fraction and aspect ratio are considered and found to be very important in diminishing the vertical displacement of the plates. Draoui *et al*. (2019) analyzed the static and dynamic behavior of CNT-reinforced composite sandwich plates. The influences of aspect ratios, volume

*Corresponding author, Ph.D.,
E-mail: selmi_fr2016@yahoo.com

ISSN: 2287-237X (Print), 2287-2388 (Online)

fraction, types of reinforcement and plate thickness on the bending and vibration analyses of CNT-reinforced composite sandwich plates were studied and discussed. It was suggested that the face sheet reinforced sandwich plate has a high resistance against deflections compared to other types of reinforcement. The vibration response of the double walled carbon nanotubes for various boundary conditions was studied by Ravi (2018). The influence of Winkler elastic medium on vibration frequency and the exceptional dynamic properties of carbon nanotubes were reported. Ebrahimi and Mahmoodi (2018) examined the thermal effect on free vibration characteristics of cracked carbon nanotubes (CNT). The influences of different parameters like crack severity, temperature change and the number of cracks on the system frequencies were investigated. Semmah *et al*. (2019) studied the thermal buckling characteristics of zigzag SWNT embedded in a one-parameter elastic medium. This model can take into account the transverse shear deformation effects of nanotubes. The effect of Winkler elastic foundation modulus, the ratio of the length to the diameter, the transverse shear deformation and rotary inertia on the critical buckling temperature were discussed. Bouadi *et al*. (2018) used new nonlocal higher order shear deformation theory to study the buckling properties of single graphene sheet. Closed-form solutions for critical buckling forces of the graphene sheets are obtained and influences of length, thickness of the graphene sheets and shear deformation on the critical buckling force have been examined. Karami *et al*. (2019) studied the forced resonance vibration of Functionally Graded Polymer Composite nanoplates reinforced with Graphene Nano-Platelets (GNPs). The influences of the GNPs distribution schemes, nonlocal and strain gradient length scale parameters, weight fraction and the total number of layers of GNPs as well as geometrically parameters were discussed in detail. The results show that the impact of layer's number on the resonance position depends on the reinforcement patterns. The work of Rakrak *et al*. (2019) was concerned with the free vibration problem for chiral double-walled carbon nanotube. They have presented the significant effect of the aspect ratio, the vibrational mode number, the small-scale coefficient and chirality of double-walled carbon nanotube on the frequency ratio of carbon nanotubes. Hajmohammad *et al*. (2018) applied a layerwise shear deformation theory to analyze the buckling of piezoelectric truncated conical shell which core is a multiphase nanocomposite reinforced by CNT and carbon fibers. The influences of CNT weight percent and other variables on the buckling load of the smart structure are presented. It was shown that increasing the CNTs weight percent increases the buckling load.

As explained previously, various investigations on the dynamic behavior of intact and cracked Al-alloy structural elements were carried out. The fracture mechanisms of Al-alloy structures were identified and the higher strength that they possess was proved but its fracture toughness was shown to be poor.

This study aims to test the capability of SWNT in reducing the effect of cracks on the dynamic behavior of Al-alloy.

The paper has the following outline. In section 2, the Mori-Tanaka homogenization technique is briefly presented. Section 3 details the modal strain energy based method. Section 4 presents the numerical results of free vibration of cantilever SWNT/Al-alloy composite beams. The effect of SWNT volume fraction, SWNT aspect ratio, crack depth and crack location on the dynamic behavior of intact and cracked composite beams is discussed on the same section 4. Lastly, Section 5 summarizes the results and conclusions.

2. Mori-Tanaka approach

Different micromechanical approaches have been proposed in the literature to determine the effective mechanical properties of heterogeneous materials. Among these approaches, the Mori-Tanaka scheme is the most popularly used. It is based on ensemble volume average method and is mainly used for moderate inclusion volume fraction (Selmi *et al*. 2007, Doghri and Ouaar 2003).

The Mori-Tanaka method is selected due to its simplicity and its applicability to diverse heterogeneous material systems (Mori and Tanaka 1973, Benveniste 1987). For composites comprising two phases; the matrix with a corresponding stiffness C_m and volume fraction V_m, while the reinforcement phase has a stiffness C_r and a volume fraction V_r, the expression for the strain-concentration factor is given as

$$A = [I + SC_m^{-1}.(C_r - C_m)]^{-1} \quad (1)$$

Where I is the fourth order identity tensor and S is the standard Eshelby tensor. The effective composite stiffness C is given as follow

$$C = C_m + V_r \langle (C_r - C_m).A \rangle .[V_m I + V_r \langle A \rangle]^{-1} \quad (2)$$

where < . > represent the orientational average

Here, the two-level procedure, Friebel *et al*. (2006), is used. In the first level each SWNT (graphene sheet with cavities) is homogenized. The homogenized SWNT plays the role of a homogeneous reinforcement for Al-alloy matrix. Choosing Mori-Tanaka (M–T) for both levels, the scheme is labeled "two-level(M–T/M–T)".

3. Modal strain energy based method

Fig. 1 shows an Euler-Bernoulli cantilever beam of length, L, height, H, and width B, containing an edge crack of depth, a, and located at the position, L_1, from the fixed support. The crack is supposed to remain open during vibrations. The Young's modulus, the Poisson's ratio and the mass density of SWNT/Al-alloy composite materials are respectively denoted by, E, ρ and ν.

For the convenience of deduction and calculation, the dimensionless parameters are defined

$$u = {}^{x}/_{L},\ h = {}^{H}/_{L},\ b = {}^{B}/_{L},\ \alpha = {}^{a}/_{H},\ e = {}^{L_1}/_{L}$$

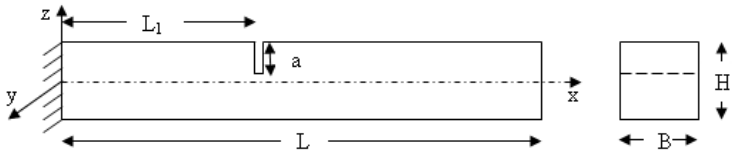

Fig. 1 An Euler-Bernoulli cantilever beam model with an edge crack

Assuming no volume changes due to the crack, the fractional changes in modal strain energy can be related to the fractional changes in frequency as proposed by Gudmundson (1992)

$$f_{ci}^2 = f_i^2\left(1 - \frac{\Delta MSE_i}{MSE_i}\right) \quad (3)$$

where f_i and f_{ci} are the angular eigenfrequencies before and after the crack occurrence, and the subscript, i, denotes the i^{th} mode.

For Euler-Bernoulli beam theory, the i^{th} modal strain energy MSE_i can be written as Kim and Stubbs (2003)

$$MSE_i = \frac{1}{2}E\left(\frac{bh^3}{12}\right)\int_0^1 \left[\phi_i''(u)\right]^2 du \quad (4)$$

where ϕ_i is the i^{th} mode shape.

The energy loss rate of the i^{th} modal strain energy is (Anderson 2005)

$$\frac{\partial(\Delta MSE_i)}{\partial a} = B\frac{(1-\nu^2)}{E}K_I^2 \quad (5)$$

The stress intensity factor K_I can be given as (Chondros *et al*. 1998)

$$K_I = \sigma\sqrt{\pi a}F_I(\alpha) \quad (6)$$

The term $F_I(\alpha)$ is a geometrical factor depending on α (Kim and Stubbs 2003)

$$F_I(\alpha) = 1.122 - 1.40\alpha + 7.33\alpha^2 - 13.08\alpha^3 + 14\alpha^4 \quad (7)$$

The stress level is given by

$$\sigma(u) = \frac{1}{2}Eh\phi_i'' \quad (8)$$

Substituting Eqs. (6)-(8) into Eq. (5), the developed expression of the decrease of modal strain energy is

$$\Delta MSE_i = \frac{(1-\nu^2)Ebh^4\pi\alpha^2F_I^2(\alpha)}{8}\left[\phi_i''(u)\right]^2\Big|_{u=e} \quad (9)$$

From Eqs. (4) and (11), the following equation can be derived

$$\frac{\Delta MSE_i}{MSE_i} = 3h\pi\alpha^2(1-\nu^2)F_I^2(\alpha)\frac{\left[\phi_i''(u)\right]^2\Big|_{u=e}}{\int_0^1[\phi_i''(u)]^2\,du} = \frac{3(1-\nu^2)H\pi\alpha^2F_I^2(\alpha)}{L}\frac{\left[\phi_i''(u)\right]^2\Big|_{u=e}}{\int_0^1[\phi_i''(u)]^2\,du} \quad (10)$$

Knowing the fractional changes in modal strain energy, the angular eigenfrequencies after the crack occurrence can be gotten from Eq. (1).

The mode shape of an Euler-Bernoulli cantilever beam is given as

$$\phi_i = c_i[sin(\beta_i u) - sinh(\beta_i u)] + cos(\beta_i u) - cosh\,s\,(\beta_i u) \quad (11)$$

With $\beta_1 = 1.875104$, $\beta_2 = 4.69409, \beta_i = (i - {}^1/_2)\pi$ and $c_i = \frac{sin(\beta_i) - sinh(\beta_i)}{cos(\beta_i) + cosh(\beta_i)}$

4. Numerical results

4.1 Validation against other methods

Results delivered by the presented formulation are validated against those obtained by finite element, experiment, dynamic stiffness theory and other approaches (Kisa *et al*. 1998, Banerjee and Guo 2009, Chen *et al*. 2013).

For the comparison with Kisa *et al*. (1998) and Banerjee and Guo (2009), the data used for the analysis are as follows: L = 0.2 m, B = 0.025 m, H = 0.0078 m, $E = 216\,GPa$, $\nu = 0.28$ and $\rho = 7850\,Kg/m^3$. Those used to perform the comparison with Chen *et al*. (2013) are: L = 0.48 m, B = 0.01 m, H = 0.0044 m, $E = 196\,GPa$, $\nu = 0.3$ and $\rho = 7860\,Kg/m^3$.

Tables 1-3 show the comparison between the presented method and other approaches.

Interpretation: From Tables 1-3, it can be noted that the numerical results obtained from the presented method show good agreement with previously published results. The satisfactory results concerning the frequency parameters give confidence in the predictions reported in next sections.

4.2 Parametric study

The method described in the previous section has been applied to cracked Euler Bernoulli beams for which the dimensions are chosen as: B = 35 cm and H = 70 cm.

The Young's modulus, the Poisson's ratio and the density of Al-alloy taken in this paper are; $E_m = 70\,GPa$, $\nu_m = 0.33$ and $\rho_m = 2700\,Kg/m^3$, respectively (Zainuddin and Ali 2016) while the Young's modulus and the Poisson's ratio of the SWNT are $E_r = 2520GPa$ and $\nu_m = 0.25$, respectively (Selmi *et al*. 2007). The density of the armchair SWNT with chiral index of (10, 10) is $\rho_r = 1330\,Kg/m^3$ (Eatemadi *et al*. 2014).

Table 1 Natural frequencies (Hz) for different crack locations (α = 0.5)

Method	e	0,167	0,271	0,375	0,479	0,583	0,687	0,792
Present	ω1	14,580	14,859	15,073	15,225	15,322	15,376	15,399
	ω2	96,151	96,152	94,091	92,288	92,311	93,925	95,672
	ω3	269,176	260,810	262,834	270,103	265,409	256,692	260,773
Experiment (Chen *et al*. 2013)	ω1	15,140	15,225	15,280	15,320	15,350	15,370	15,386
	ω2	96,360	96,390	95,820	95,210	95,420	95,720	96,420
	ω3	268,720	266,610	267,400	271,180	268,610	266,190	267,470
Ansys (Chen *et al*. 2013)	ω1	15,144	15,230	15,297	15,356	15,383	15,405	15,418
	ω2	96,383	96,416	95,802	95,209	95,235	95,680	96,211
	ω3	269,810	267,380	267,910	270,030	268,580	266,050	267,080
Theory (Chen *et al*. 2013)	ω1	14,980	15,120	15,230	15,310	15,360	15,380	15,400
	ω2	96,340	96,340	95,260	94,340	94,330	95,130	96,070
	ω3	269,720	265,440	266,500	270,210	267,780	263,420	265,210

Table 2 Natural frequencies (Hz) for different crack depths and different locations

Method	e	0,167		0,792	
	α	0,3	0,5	0,3	0,5
Present	ω1	15,241	14,580	15,404	15,399
	ω2	96,463	96,151	96,367	95,672
	ω3	270,090	269,176	268,412	260,773
Experiment (Chen *et al*. 2013)	ω1	15,360	15,140	15,430	15,386
	ω2	96,720	96,470	96,590	96,420
	ω3	270,310	269,720	269,340	267,470
Ansys (Chen *et al*. 2013)	ω1	15,332	15,144	15,413	15,418
	ω2	96,470	96,383	96,420	96,211
	ω3	270,020	269,810	269,250	267,080
Theory (Chen *et al*. 2013)	ω1	15,280	14,980	15,400	15,400
	ω2	96,490	96,340	96,410	96,070
	ω3	270,140	269,720	268,860	265,210

Table 3 Natural frequencies for different crack depths and different locations

		ω_1(rad/s)			ω_2(rad/s)			ω_3(rad/s)		
E	α	Present	Banerjee and Guo 2009	Kisa *et al.* 1998	present	Banerjee and Guo 2009	Kisa *et al.* 1998	Present	Banerjee and Guo 2009	Kisa *et al.* 1998
0,2	0,2	1021,664	-	1020,137	6505,413	-	6457,396	18132,452	-	17872,91
	0,4	940,126	-	966,953	6500,911	-	6454,483	17725,525	-	17596,57
0,4	0,2	1031,559	1031,800	1030,095	6438,083	6441,3	6389,394	18094,723	18098	17844,86
	0,4	999,743	1010,856	1006,100	6107,480	6237,0	6174,539	17504,694	17740	17499,83
0,6	0,2	1036,564	1036,600	1035,284	6414,401	6419,0	6365,914	18065,965	18070	17807,94
	0,4	1028,787	1030,900	1029,262	5963,958	6139,9	6071,655	17334,795	17633	17359,27

The variation of the Normalized first three natural frequencies, (ω_n/ω_{n0}), of SWNT/Al-alloy composite beams as a function of the crack position L_1/L for various crack thickness a/h and SWNT aspect ratios is depicted in Figs. 2 and 3. For this set of results the SWNT volume fraction is taken equal to 1%.

The next two sets of results (Figs. 4-5 and 6-7) was obtained to demonstrate the effect of crack depth a/h and

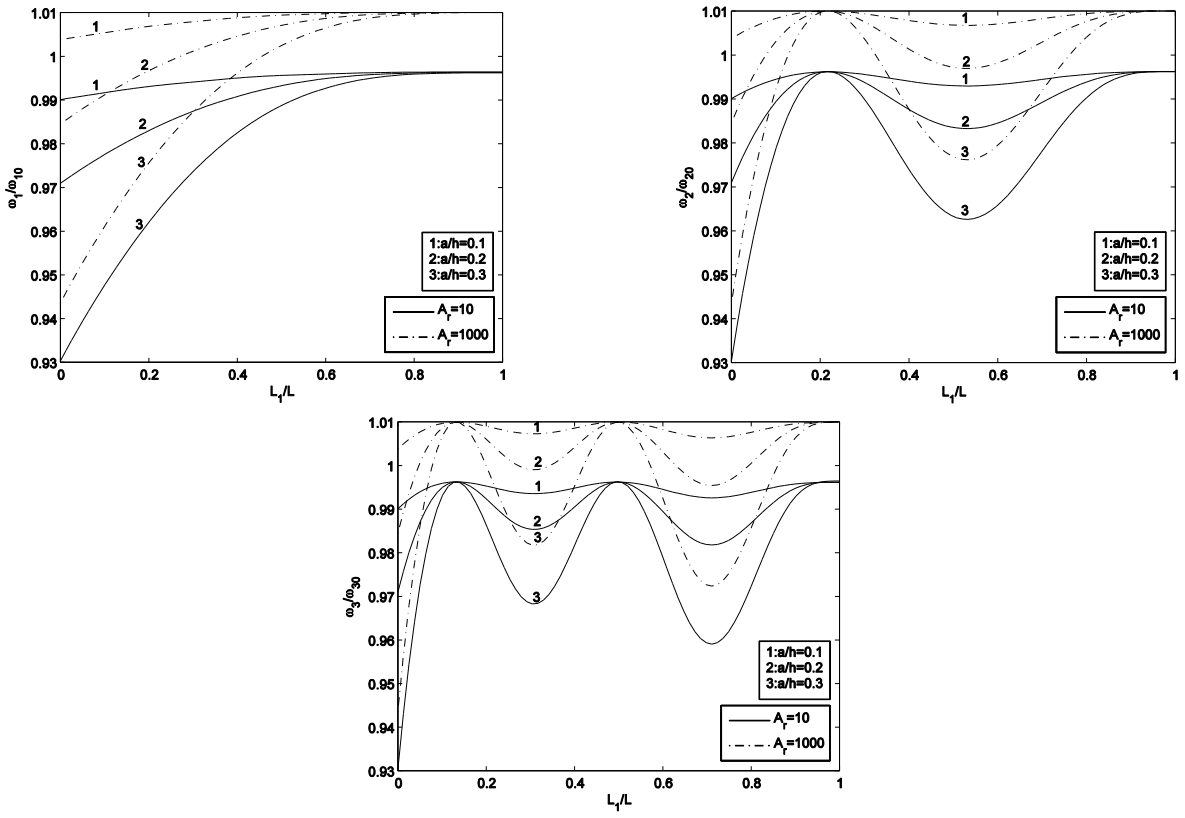

Fig. 2 Effect of crack depth ratio on the first three normalized frequencies of SWNT/Al_2O_3 beams for v = 1%

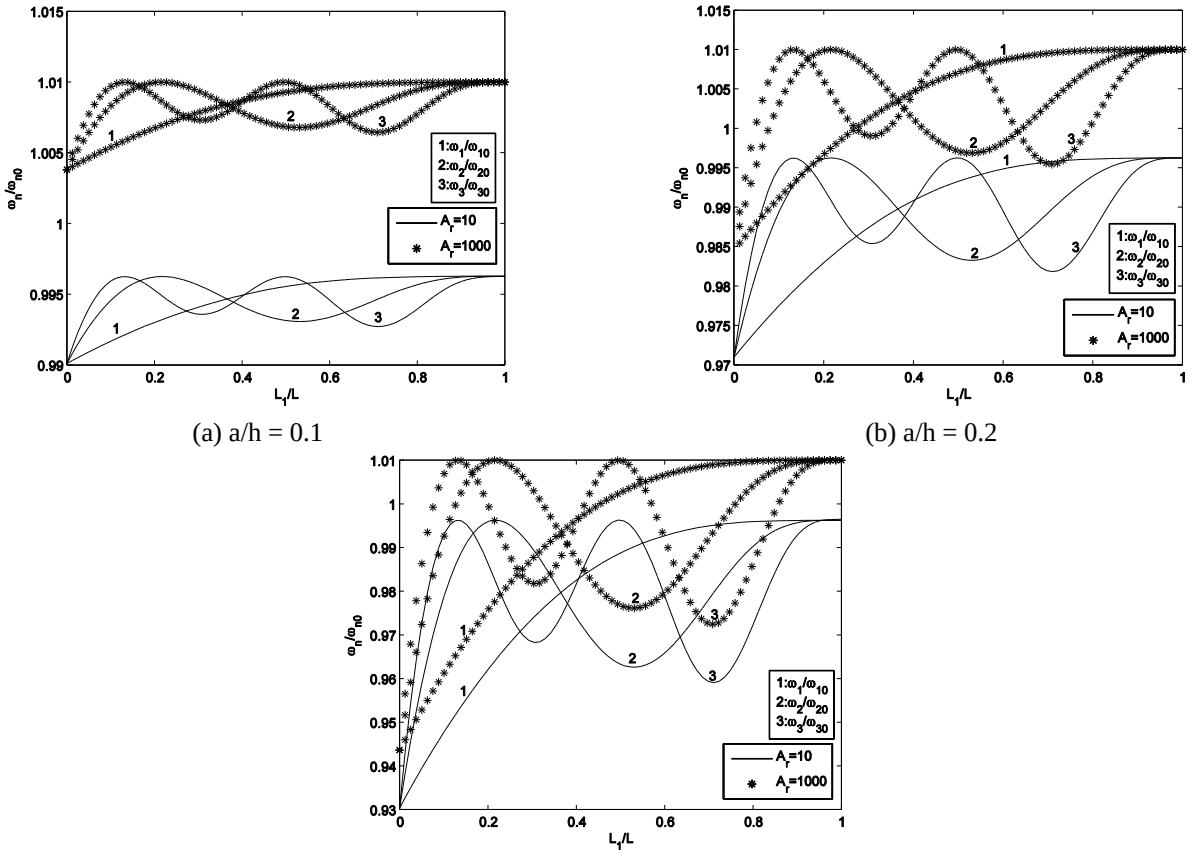

(a) a/h = 0.1

(b) a/h = 0.2

(c) a/h = 0.3

Fig. 3 Effect of SWNT aspect ratio on the first three normalized frequencies of cracked SWNT/Al_2O_3 beams for v = 1%

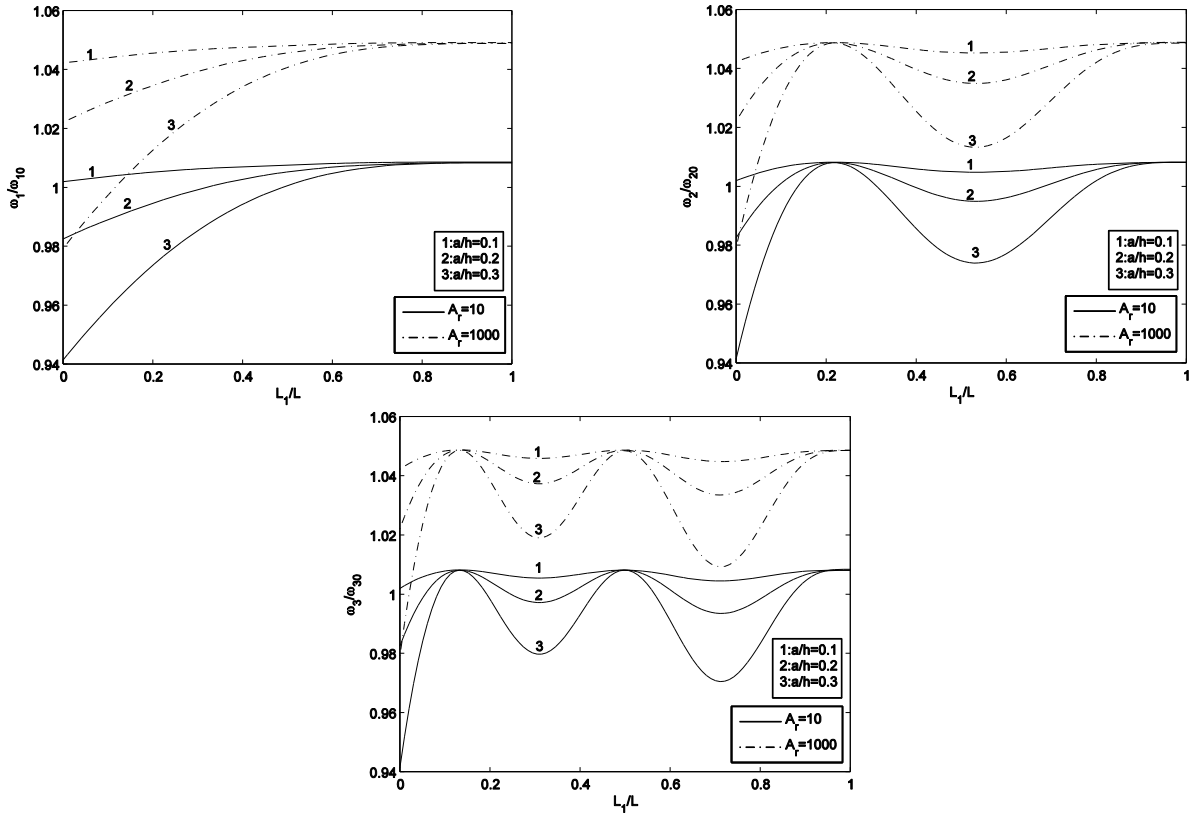

Fig. 4 Effect of crack depth on the first three normalized frequencies of SWNT/Al_2O_3 beams for v = 5%

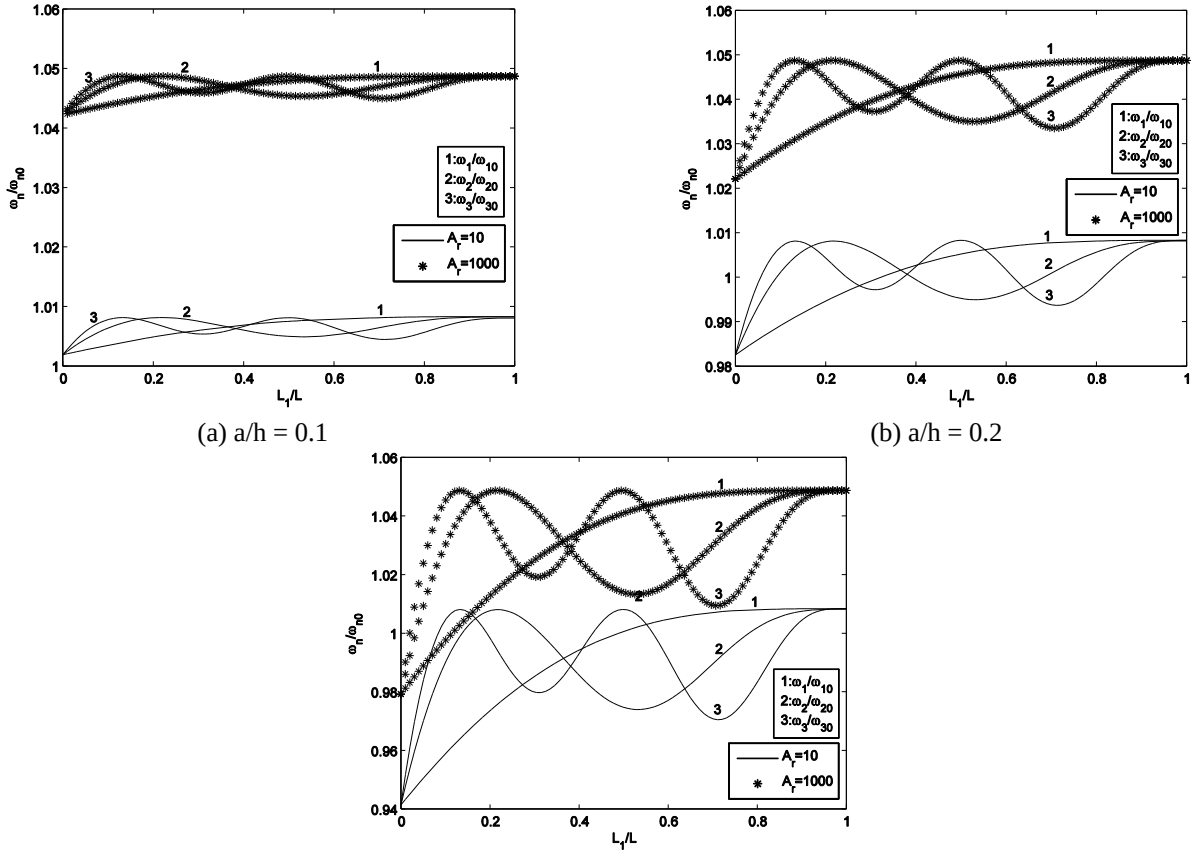

(a) a/h = 0.1 (b) a/h = 0.2

(c) a/h = 0.3

Fig. 5 Effect of SWNT aspect on the first three normalized frequencies of SWNT/Al_2O_3 beams for v = 5%

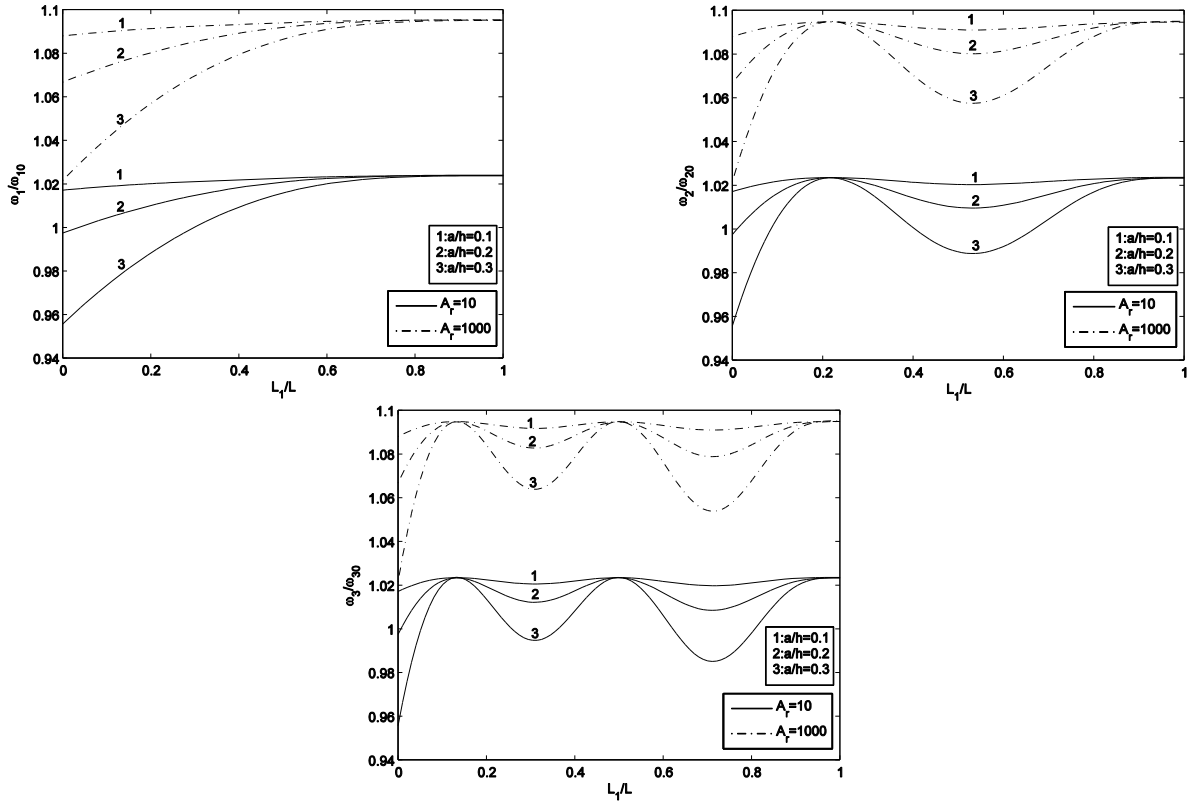

Fig. 6 Effect of crack depth ratio on the first three normalized frequencies of SWNT/Al_2O_3 beams for v = 10%

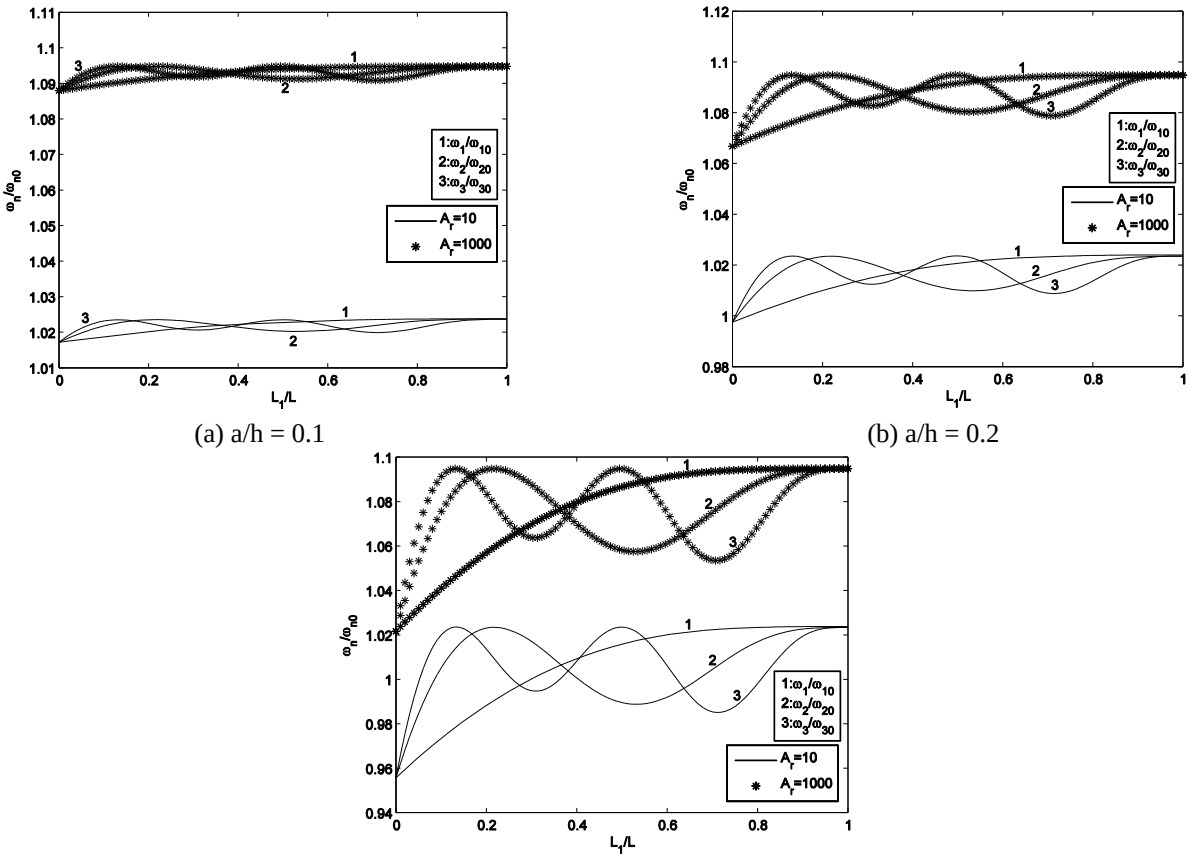

(a) a/h = 0.1 (b) a/h = 0.2

(c) a/h = 0.3

Fig. 7 Effect of SWNT aspect ratio on the first three normalized frequencies of SWNT/Al_2O_3 beams for v = 10%

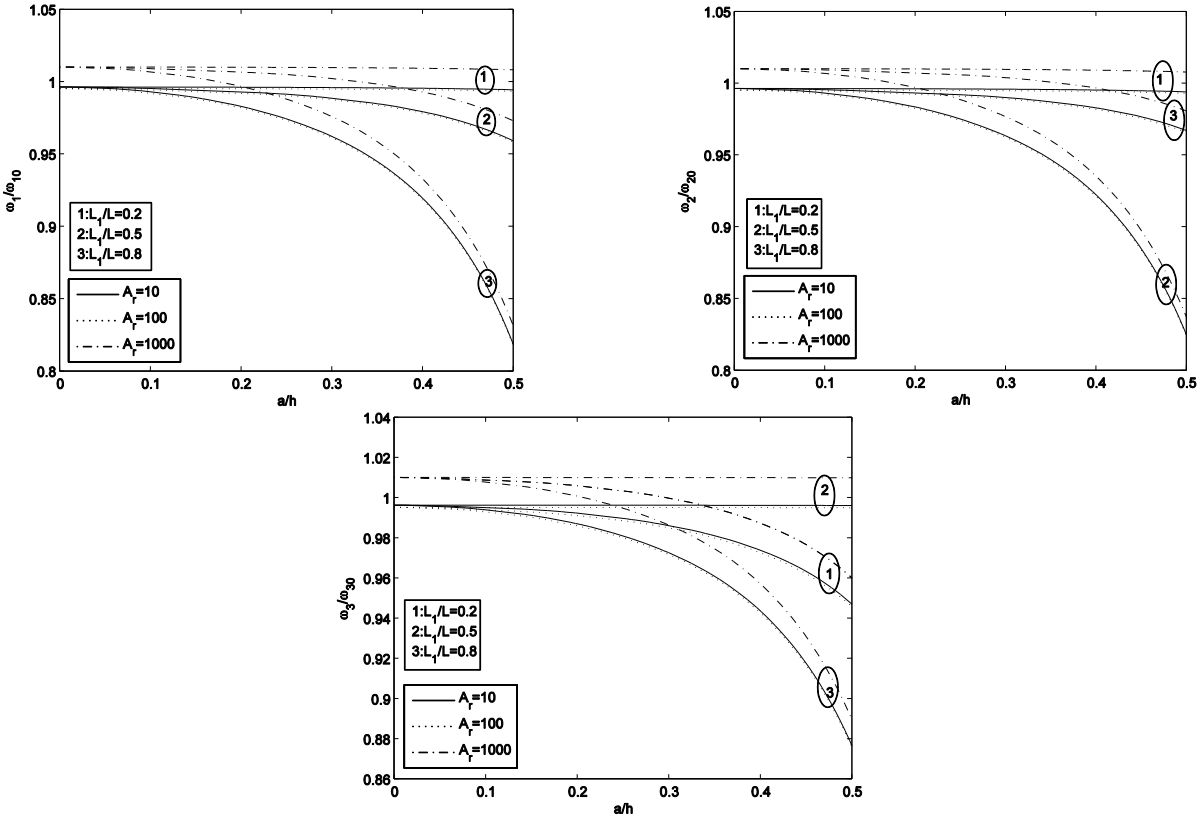

Fig. 8 Effect of damage location on the first three normalized frequencies of SWNT/Al_2O_3 beams for v = 1%

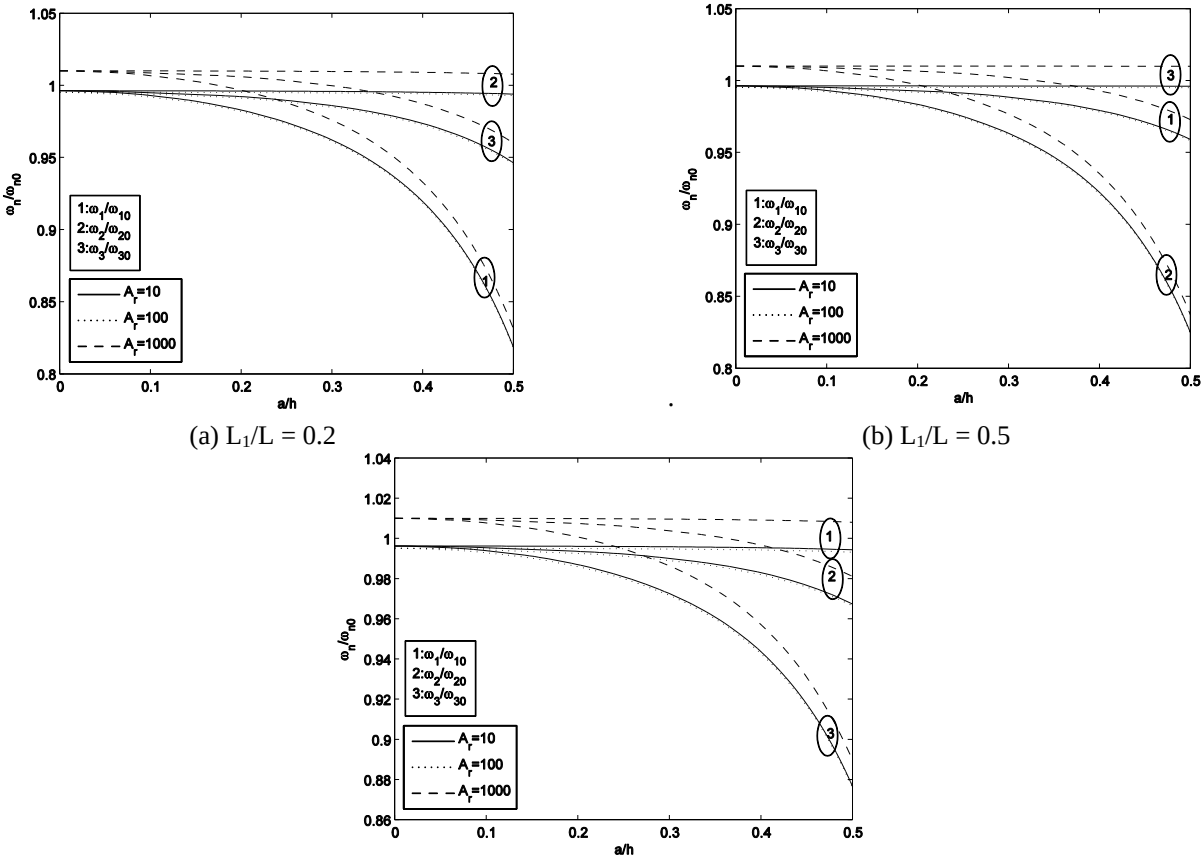

(a) L_1/L = 0.2 (b) L_1/L = 0.5

(c) L_1/L = 0.8

Fig. 9 Effect of SWNT aspect ratio on the first three normalized frequencies of SWNT/Al_2O_3 beams for v = 1%

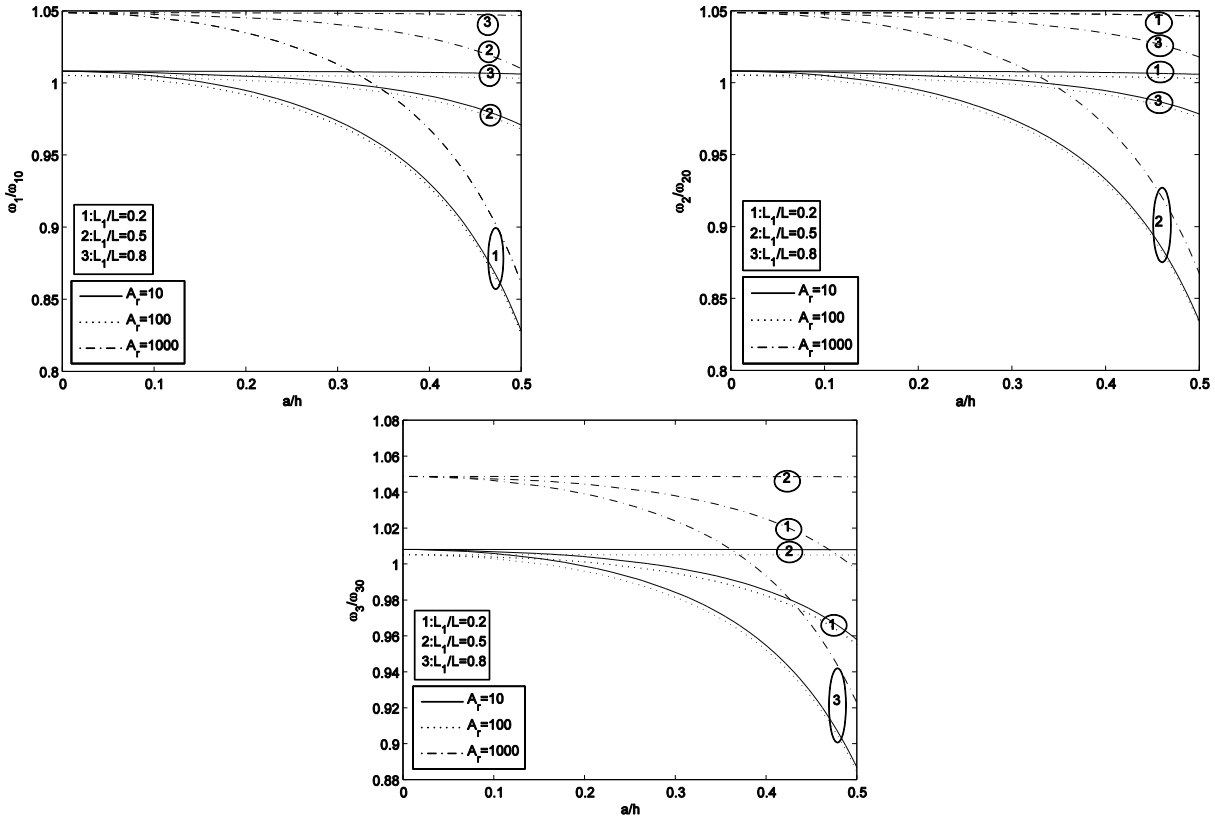

Fig. 10 Effect of damage location on the first three normalized frequencies of SWNT/Al_2O_3 beams for v = 5%

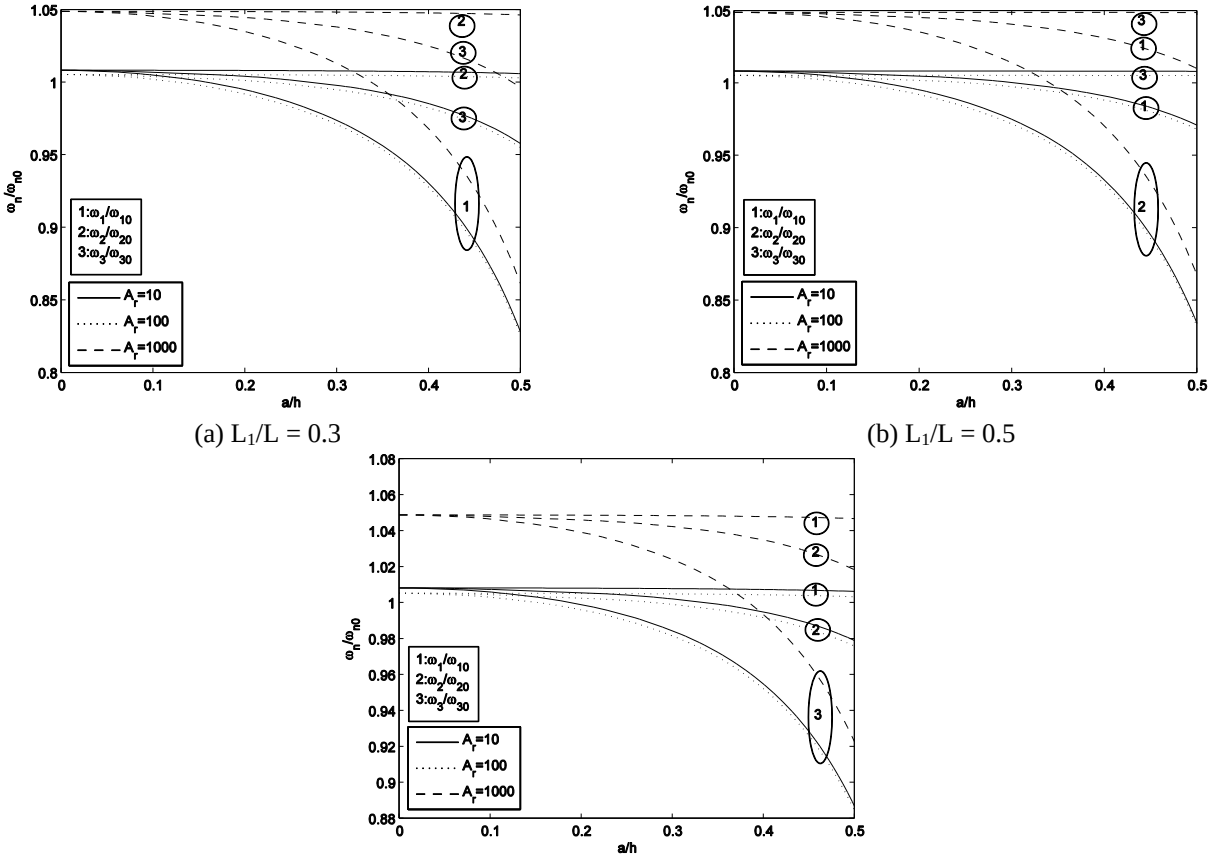

(a) L_1/L = 0.3 (b) L_1/L = 0.5

(c) L_1/L = 0.8

Fig. 11 Effect of SWNT aspect ratio on the first three normalized frequencies of SWNT/Al_2O_3 beams for v = 5%

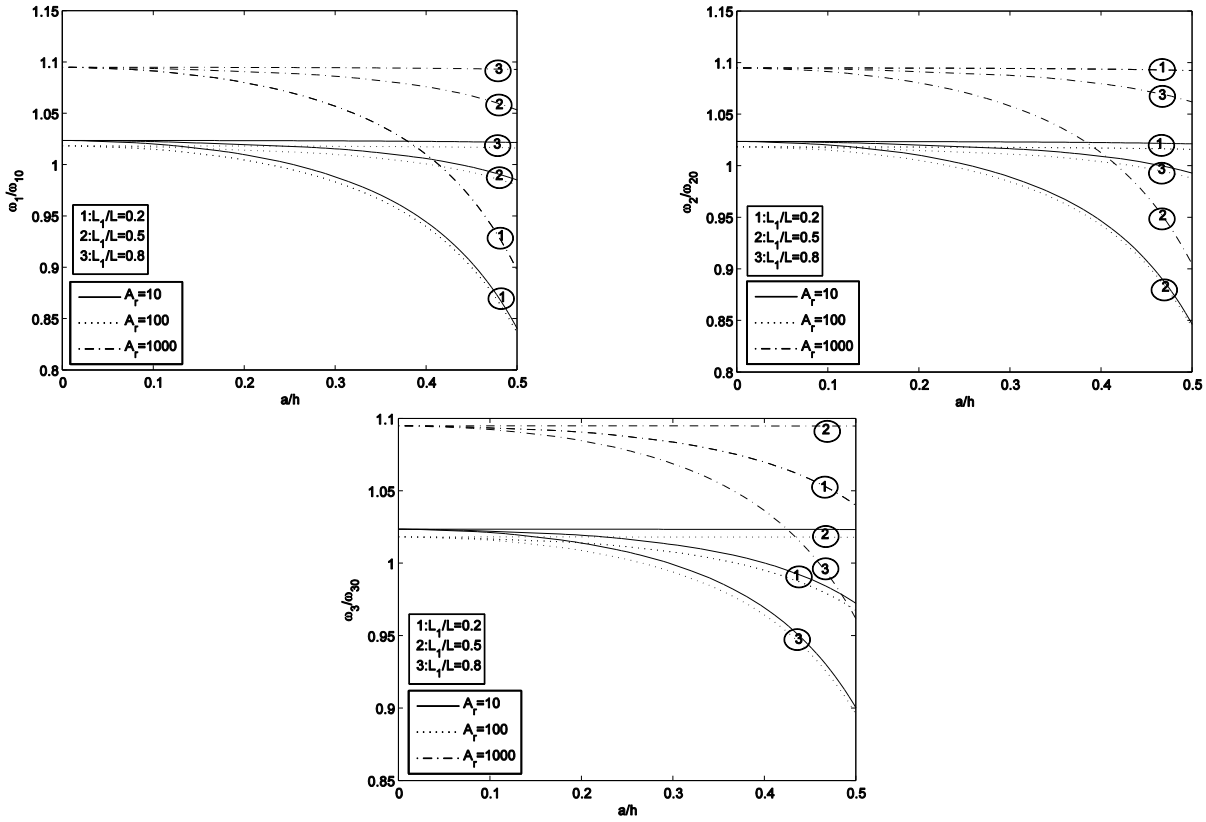

Fig. 12 Effect of damage location on the first three normalized frequencies of SWNT/Al_2O_3 beams for v = 10%

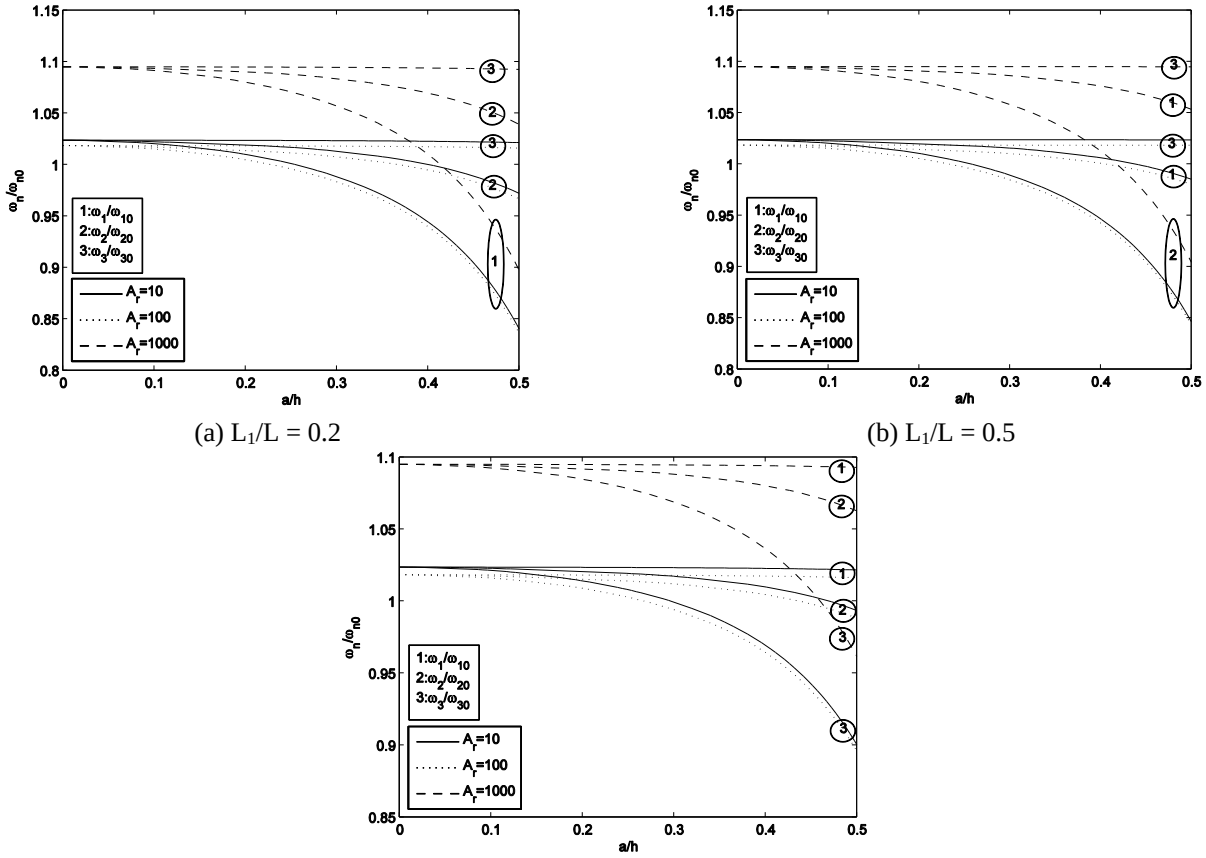

(a) L_1/L = 0.2

(b) L_1/L = 0.5

(c) L_1/L = 0.8

Fig. 13 Effect of SWNT aspect ratio on the first three normalized frequencies of SWNT/Al_2O_3 beams for v = 10%

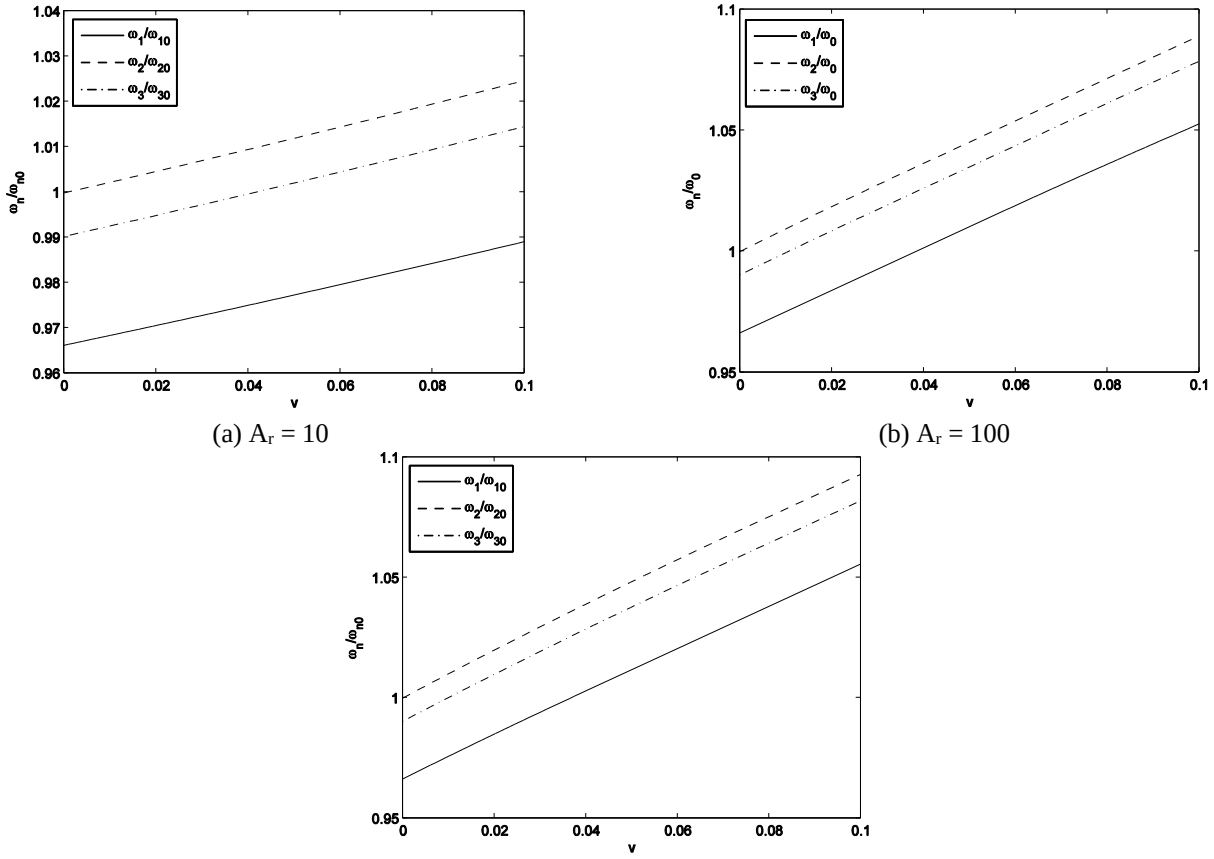

(a) $A_r = 10$ (b) $A_r = 100$

(c) $A_r = 1000$

Fig. 14 Variation of the first three normalized frequencies of SWNT/Al_2O_3 beams as a function of SWNT volume fraction

SWNT aspect ratio on the first three normalized natural frequencies of cracked composite beams for SWNT volume fraction equal to 5% and 10%, respectively.

It is clearly shown that the evolution of each normalized natural frequency as a function of crack position has its proper shape. The common point between these shapes is the horizontal asymptotic that they present from L_1/L close to 0.9.

One can observe from Figs. 3, 5 and 7 that independently of crack geometry characteristics and SWNT volume fraction, all three natural frequencies increase with the same fashion when increasing the SWNT aspect ratio.

For a given L_1/L less than 0.9, increasing a/h reduces the normalized natural frequencies. This drop is spectacular for cracks close to the fixed support. Figs. 2, 4 and 6 show that the decrease of natural frequencies due to crack of depth ratio a/h = 0.1 can be compensated with just 1% SWNT volume fraction.

The variation of the Normalized first three natural frequencies ω_n/ω_{n0} of SWNT/Al-alloy composite beams according to a/h for various values of $L_1/L$and SWNT aspect ratios is represented in Figs. 8 and 9. The SWNT volume fraction is taken equal to 1%.

The next two sets of results (Figs. 10-11 and 12-13) was obtained to clarify the effect of particular values of $L_1/L$and SWNT aspect ratios on the first three normalized natural frequencies of cracked composite beams for SWNT volume fraction equal to 5% and 10%, respectively.

It can be clearly seen that the three normalized natural frequency versus a/h have the same trend regarding to the three volume fraction (1%, 5% and 10%).

It is noted that for superficial cracks of a/h small than 0.1, Small content of short SWNT can recover the decrease in natural frequencies.

Figs. 9, 11 and 13 show that the effect of a/h on the natural frequencies depends on the crack position; for$L_1/L = 0.2$, ω_2/ω_{20}does not changes too much but ω_1/ω_{10} decreases rapidly. For $L_1/L = 0.1$it isω_3/ω_{30} which seems to be constant and the ω_2/ω_{20}decreases rapidly. Finally, for $L_1/L = 0.8$ the change of ω_2/ω_{20} is negligible and the decrease of ω_3/ω_{30} is remarkable. Whatever the value of L_1/L the decrease becomes more visible for deep cracks.

Fig. 14 illustrates the variation of the normalized natural frequency of SWNT/Al-alloy cantilever beams as a function of the volume fraction for several aspect ratios, $L_1/L =$ 0.2and a/h = 0.3

It can be noted that small quantity of SWNT can eliminate the effect of deep crack on the natural frequencies.

With regard to the effect of aspect ratio on natural frequencies, the previous figures has shown that short fibers will have much smaller effect than long ones. This is obvious since increasing the aspect ratio increases towards the composite Young's modulus.

5. Conclusions

The present investigation proves the capability of randomly oriented SWNT in reducing the effect of cracks on the dynamic behavior of cracked Aluminium alloy beams. This study is accomplished using micromechanical scheme and a method based on changes in modal strain energy. Results show that low concentration of short SWNT is enough to recover the decrease in natural frequencies due to cracks.

References

Anderson, T.L. (2005), *Fracture Mechanics*: *Fundamental and applications*, Third Edition. London, CRC Press, Taylor and Francis Group.

Bakhadda, B., Bachir Bouiadjra, M., Bourada, F., Bousahla, A.A., Tounsi, A. and Mahmoud, S.R. (2018), "Dynamic and bending analysis of carbon nanotube-reinforced composite plates with elastic foundation", *Wind Struct*., *Int*. *J*., **27**(5), 311-324. https://doi.org/10.12989/was.2018.27.5.311

Banerjee, J.R. and Guo, S. (2009), "On the dynamics of a cracked beam", *Proceedings of the 50th AIAA/ASME/ASCE/AHS/ASC Structures, Structural Dynamics and Materials Conference*, Palm Springs, CA, USA, May, 2429.

Benveniste, Y. (1987), "A new approach to the application of Mori-Tanaka's theory in composite materials", *Mech*. *Mater*., **6**(2), 147-157. https://doi.org/10.1016/0167-6636(87)90005-6

Borvik, T., Hopperstad, O.S. and Pedersen, K.O. (2010), "Quasi-brittle fracture during structural impact of AA7075-T651 aluminium plates", *Int*. *J*. *Impact Eng*., **37**(5), 537-551. https://doi.org/10.1016/j.ijimpeng.2009.11.001

Bouadi, A., Bousahla, A.A., Houari, M.S.A., Heireche, H. and Tounsi, A. (2018), "A new nonlocal HSDT for analysis of stability of single layer graphene sheet", *Adv*. *Nano Res*., *Int*. *J*., **6**(2), 147-162. https://doi.org/10.12989/anr.2018.6.2.147

Chen, L.H., Duan, J.W., Sun, Y. and Li, J. (2013), "The study of the Vibration Characteristics of the Cantilever Beam with a Surface Crack", *Appl*. *Mech*. *Mater*., **394**(C), 121-127. https://doi.org/10.4028/www.scientific.net/AMM.394.121

Chondros, T., Dimarogonas, A. and Yao, J. (1998), "A continuous cracked beam vibration theory", *J*. *Sound Vib*., **215**(1), 17-34. https://doi.org/10.1006/jsvi.1998.1640

Doghri, I. and Ouaar, A. (2003), "Homogenization of two-phase elasto-plastic composite materials and structures: Study of tangent operators, cyclic plasticity and numerical algorithms", *Int*. *J*. *Solids Struct*., **40**(7), 1681-1712. https://doi.org/10.1016/S0020-7683(03)00013-1

Draoui, A., Zidour, M., Tounsi, A. and Adim, B. (2019), "Static and dynamic behavior of nanotubes-reinforced sandwich plates using (FSDT)", *J*. *Nano Res*., **57**, 117-135. https://doi.org/10.4028/www.scientific.net/JNanoR.57.117

Duan, F., Liu, J., Wang, G. and Yu, Z. (2018), "Dynamic behaviour of aluminium alloy plates with surface cracks subjected to repeated impacts", *Ships Offshore Struct*., **14**(5), 478-491. https://doi.org/10.1080/17445302.2018.1507088

Dumont, D., Deschamps, A. and Brechet, Y. (2003), "On the relationship between microstructure, strength and toughness in AA7050 aluminum alloy", *Mater*. *Sci*. *Eng*., **356**(2), 326-336. https://doi.org/10.1016/S0921-5093(03)00145-X

Eatemadi, A., Daraee, H., Karimkhanloo, H., Kouhi, M., Zarghami, N., Akbarzadeh, A., Abasi, M., Hanifehpour, Y. and Joo, S.W. (2014), "Carbon nanotubes: properties, synthesis, purification, and medical applications", *Nanoscale Res*. *Lett*., **9**, 393. https://doi.org/10.1186/1556-276X-9-393

Ebrahimi, F. and Mahmoodi, M. (2018), "Vibration analysis of carbon nanotubes with multiple cracks in thermal environment", *Adv*. *Nano Res*., *Int*. *J*., **6**(1), 57-80. https://doi.org/10.12989/anr.2018.6.1.057

Friebel, C., Doghri, I. and Legat, V. (2006), "General mean-field homogenization schemes for viscoelastic composites containing multiple phases of coated inclusions", *Int*. *J*. *Solids Struct*., **43**(9), 2513-2541. https://doi.org/10.1016/j.ijsolstr.2005.06.035

Gudmundson, P. (1982), "Eigenfrequency changes of structures due to cracks, notches or other geometrical changes", *J*. *Mech*. *Phys*. *Solids*, **30**(5), 339-353. https://doi.org/10.1016/0022-5096(82)90004-7

Hajmohammad, M.H., Zarei, M.S., Farrokhian, A. and Kolahchi, R. (2018), "A layerwise theory for buckling analysis of truncated conical shells reinforced by CNTs and carbon fibers integrated with piezoelectric layers in hygrothermal environment", *Adv*. *Nano Res*, *Int*. *J*., **6**(4), 299-321. https://doi.org/10.12989/anr.2018.6.4.299

Han, N.M., Zhang, X.M., Liu, S.D., Ke, B. and Xin, X. (2011), "Effects of pre-stretching and aging on the strength and fracture toughness of aluminium alloy 7050", *Mater*. *Sci*. *Eng*. *A*, **528**(10-11), 3714-3721. https://doi.org/10.1016/j.msea.2011.01.068

Heshmati, M. and Yas, M.H. (2013), "Free vibration analysis of functionally graded CNT-reinforced nanocomposite beam using Eshelby-Mori-Tanaka approach", *J*. *Mech*. *Sci*. *Technol*., **27**(11), 3403-3408. https://doi.org/10.1007/s12206-013-0862-8

Karami, B., Shahsavari, D., Janghorban, M. and Tounsi, A. (2019), "Resonance behavior of functionally graded polymer composite nanoplates reinforced with grapheme nanoplatelets", *Int*. *J*. *Mech*. *Sci*., **156**, 94-105. https://doi.org/10.1016/j.ijmecsci.2019.03.036

Kim, J. and Stubbs, N. (2003), "Crack detection in beam-type structures using frequency data", *J*. *Sound Vib*., **259**(1), 145-160. https://doi.org/10.1006/jsvi.2002.5132

Kisa, M., Brandon, J. and Topcu, M. (1998), "Free vibration analysis of cracked beams by a combination of finite elements and component mode synthesis methods", *Comput*. *Struct*., **67**(4), 215-223. https://doi.org/10.1016/S0045-7949(98)00056-X

Liu, R.P., Dong, Z.J. and Pan, Y.M. (2006), "Solidification crack susceptibility of aluminum alloy weld metals", *Transact*. *Nonferrous Metals Soc*. *China*, **16**(1), 110-116. https://doi.org/10.1016/S1003-6326(06)60019-8

Mori, T. and Tanaka, K. (1973), "Average stress in matrix and average elastic energy of materials withmisfitting inclusions", *Acta Metallurgica*, **21**, 571-574. https://doi.org/10.1016/0001-6160(73)90064-3

Mostafavi, M., Smith, D.J. and Pavier, M.J. (2011), "Fracture of aluminium alloy 2024 under biaxial and triaxial loading", *Eng*. *Fract*. *Mech*., **78**(8), 1705-1716. https://doi.org/10.1016/j.engfracmech.2010.11.006

Nejati, M., Eslampanah, A. and Najafizadeh, M.H. (2016), "Buckling and vibration analysis of functionally graded carbon nanotube-reinforced beam under axial load", *Int*. *Appl*. *Mech*., **8**(1), 1650008. https://doi.org/10.1142/S1758825116500083

Pedersen, K.O., Borvik, T. and Hopperstad, O.S. (2011), "Fracture mechanisms of aluminium alloy AA7075-T651 under various loading conditions", *Mater*. *Des*., **32**(1), 97-107. https://doi.org/10.1016/j.matdes.2010.06.029

Rahbar-Ranji, A. and Zarookian, A. (2015), "Ultimate strength of stiffened plates with a transverse crack under uniaxial compression", *Ships Offshore Struct*., **10**(4), 416-425. https://doi.org/10.1080/17445302.2014.942078

Rakrak, K., Zidour, M., Heireche, H., Bousahla, A.A. and Chemi, A. (2019), "Free vibration analysis of chiral double-walled carbon nanotube using non-local elasticity theory", *Adv*. *Nano*

Res., *Int. J*., **4**(1), 31-44. https://doi.org/10.12989/anr.2016.4.1.031

Ravi, K. (2018), "Investigation on mechanical vibration of double-walled carbon nanotubes with inter-tube Van der waals forces", *Adv. Nano Res*., *Int. J*., **6**(2), 135-145. https://doi.org/10.12989/anr.2018.6.2.135

Selmi, A. and Bisharat, A. (2018), "Free vibration of functionally graded SWNT reinforced aluminum alloy beam", *J. Vibroeng*., **20**(5), 2151-2164. https://doi.org/10.21595/jve.2018.19445

Selmi, A., Friebel, C., Doghri, I. and Hassis, H. (2007), "Prediction of the elastic properties of single walled carbon nanotube reinforced polymers: A comparative study of several micromechanical models", *Compos. Sci. Technol*., **67**(10), 2071-2084. https://doi.org/10.1016/j.compscitech.2006.11.016

Seifi, R. and Khoda-yari, N. (2011), "Experimental and numerical studies on buckling of cracked thin-plates under full and partial compression edge loading", *Thin-wall. Struct*., **49**(12), 1504-1516. https://doi.org/10.1016/j.tws.2011.07.010

Semmah, A., Heireche, H., Bousahla, A.A. and Tounsi, A. (2019), "Thermal buckling analysis of SWBNNT on Winkler foundation by non local FSDT", *Adv. Nano Res*., *Int. J*., **7**(2), 89-98. https://doi.org/10.12989/anr.2019.7.2.089

Shen, H.S. (2009), "Nonlinear bending of functionally graded carbon nanotube reinforced composite plates in thermal environments", *Compos. Struct*., **91**(1), 9-19. https://doi.org/10.1016/j.compstruct.2009.04.026

Shenas, A.G., Malekzadeh, P. and Ziaee, S. (2017), "Vibration analysis of pre-twisted functionally graded carbon nanotube reinforced composite beams in thermal environment", *Compos. Struct*., **162**, 325-340. https://doi.org/10.1016/j.compstruct.2016.12.009

Shi, X.H., Zhang, J. and Soares, C.G. (2017), "Experimental study on collapse of cracked stiffened plate with initial imperfections under compression", *Thin-wall. Struct*., **114**(C), 39-51. https://doi.org/10.1016/j.tws.2016.12.028

Xing, M.Z., Wang, Y.G. and Jiang, Z.X. (2013), "Dynamic fracture behaviors of selected aluminum alloys under three-point bending", *Defence Technol*., **9**(4), 193-200. https://doi.org/10.1016/j.dt.2013.11.002

Yas, M.H. and Samadi, N. (2012), "Free vibrations and buckling analysis of carbon nanotube-reinforced composite Timoshenko beams on elastic foundation", *Int. J. Press. Vessels Pip*., **98**, 119-128. https://doi.org/10.1016/j.ijpvp.2012.07.012

Zainuddin, H.B. and Ali, M.B. (2016), "Study of wheel rim impact test using finite element analysis", *Proceedings of Mechanical Engineering Research Day*, 141.

CC